Available online at www.sciencedirect.com
ScienceDirect
Polymer 47 (2006) 7636–7645
polymer
www.elsevier.com/locate/polymer

Cellulose-based aerogels

F. Fischer [a,*], A. Rigacci [a,*], R. Pirard [b], S. Berthon-Fabry [a], P. Achard [a]

[a] *Ecole des Mines de Paris, Center for Energy and Processes, BP 207, F-06904 Sophia Antipolis Cedex, France*
[b] *Laboratoire de Génie Chimique, Institut de Chimie, Université de Liège, B-4000 Liège, Belgium*

Received 19 April 2006; received in revised form 1 September 2006; accepted 1 September 2006
Available online 25 September 2006

Abstract

New organic aerogels were prepared using cellulose derivatives as precursors. The elaboration process and the structural characterisations of these porous cellulose-based materials are described in the present study. Series of monolithic gels were synthesised in acetone by crosslinking cellulose acetate with a non-toxic isocyanate *via* sol–gel route, using tin-based catalyst. Gelation times (ranging from 15 to 150 min) were significantly dependent on reagents' nature and concentration. Low-density materials (from 0.25 cm^3/g to 0.85 cm^3/g) were obtained after supercritical carbon dioxide drying. These newly developed nanostructured materials were characterised using mercury porosimetry, nitrogen adsorption and scanning electron microscopy. All the prepared materials have shown both a nanostructured solid network (specific surface areas between 140 and 250 m^2/g) and a nanoporous network (characteristic pore sizes between 13 and 25 nm) together with specific porous volumes as large as 3.30 cm^3/g.

Influence of sol–gel synthesis parameters as crosslinker content and cellulose degree of polymerisation or concentration was investigated. First empirical correlations between synthesis parameters and final material properties were obtained. A special attention was dedicated to the different shrinkages occurring during the elaboration process. In particular, the important shrinkage occurring during the supercritical drying step was studied in terms of affinity between the crosslinked polymeric network and carbon dioxide. In parallel, first thermo-mechanical properties were presented in terms of bulk modulus and effective thermal conductivity.

Keywords: Cellulose acetate; Aerogels; Crosslinking

1. Introduction

Many studies have already focused on aerogel-like materials because of their unique properties. Coming from soft chemistry (e.g. sol–gel), their chemical nature and nanostructuration can be tailored. For instance, chemical composition ranges from mineral to organic while internal texture can range from microporosity to macroporosity. Moreover, they can be lightweight and can present very high specific area (larger than 1000 m^2/g) with a narrow (or even broad) pore size distribution. Such structural characteristics make them potentially interesting for various applications [1].

Even if a large majority of the studies dedicated to aerogels are dealing with inorganics (SiO_2, TiO_2, ZrO_2, …), some class of organic aerogels is known to present high interest. Such materials are particularly considered as organic precursors for new family of nanostructured carbons. Most of the corresponding samples are coming from resorcinol–formaldehyde (RF) systems [2]. During the past decade, further studies on organic aerogels for thermal insulation have addressed other kinds of aerogels, mainly based on polyurethane [3,4].

Within the sphere of organic aerogels, only very few works concern the use of natural products. Knowing that cellulose is one of the most abundant natural materials, one can guess that combining sol–gel science and cellulose could be of high interest. Some works have already been devoted to the elaboration of porous cellulose via drying of physical cellulose-based gels but they are not dealing with aerogels [5–7]. Recently,

* Corresponding authors. Tel.: +33493957476; fax: +33493957535.
E-mail addresses: florent.fischer@ensmp.fr (F. Fischer), arnaud.rigacci@ensmp.fr (A. Rigacci).

0032-3861/$ - see front matter © 2006 Elsevier Ltd. All rights reserved.
doi:10.1016/j.polymer.2006.09.004

one of the first aerogel-attempt with cellulose derivatives has been published [8]. Mechanically strong nanoporous materials have been obtained.

On this basis, the present work is dedicated to the elaboration of a new class of aerogels prepared with cellulose derivatives. Our objective is to demonstrate the feasibility of a softer way and to highlight correlations between sol–gel parameters and these newly developed nanostructures.

2. Experimental

2.1. Materials

Two different cellulose acetates from Aldrich were used as polyols. They present the same acetyl content (39.8 wt% i.e. an acetyl average substitution degree of 2.4) but differ by their number-average molecular weight (M_n measured by gel permeation chromatography, equal to 30 000 and 50 000, which correspond to number-average degree of polymerisation (denoted as DP_n) respectively, equal to 110 and 190). Polymethylene polyphenylpolyisocyanate (PMDI, Lupranat® M20S, BASF) is a non-toxic polyisocyanate with an NCO content of 31.8 wt%, and was used as crosslinker. Dibutyltin dilaurate (a tin-based organometallic complex from Aldrich, denoted as DD in the following text) was used as urethane catalyst.

Reaction media were extra-dry acetone (water content inferior to 0.02 wt%). All reagents were commercially obtained and used as received without further purification.

2.2. Elaboration

Gels were prepared through a sol–gel route based on the formation of urethane bonding by polycondensation reactions between cellulose acetate (CA) and isocyanate (I) as schematically represented in Fig. 1 [9].

Cellulose acetate was first dissolved in acetone. The polymer dissolution was a two-step process at room temperature. Cellulose acetate was immersed in acetone without stirring for at least 15 h until a translucent solution is obtained. A mechanical stirring was then performed for 5 h to obtain a homogenous polymer solution. The catalyst was added under mechanical stirring. The corresponding solution was denoted as A (Fig. 2). In parallel, PMDI was dissolved in acetone with a slow mechanical stirring to obtain another solution, denoted as B. A and B were mixed by mechanical stirring for 10 min. The resulting sol was cast into different cylindrical moulds. The step-growth polymerisation leads to the gelation of the sol in the moulds. Once gelation occurred, all the cylindrical gels were kept closed and covered with an excess of acetone to prevent any evaporation. The gels were aged for seven days at room temperature. During this phase (called syneresis), the gels were washed three times with acetone in order to remove the unreacted species. Finally, the wet gels were carefully removed from the moulds for drying.

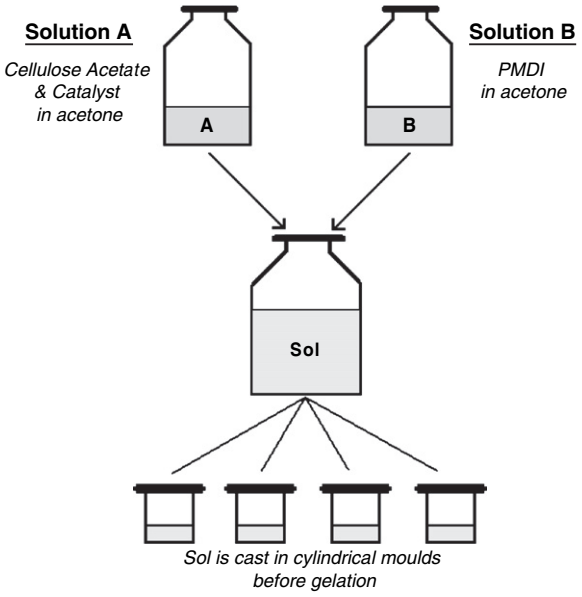

Fig. 2. Schematic presentation of the sol–gel protocol.

In a 1-l autoclave, wet gels were first washed under supercritical flow of carbon dioxide (CO_2) at 85 bars, 40 °C and 5 kg CO_2/h for 4 h. When the whole interstitial liquid phase was recovered, CO_2 was vented out slowly (0.1 bar/min) and isothermally (40 °C) to prevent any condensation phenomena [10]. Organic aerogels obtained are referenced OA1–OA5 depending on their formulation.

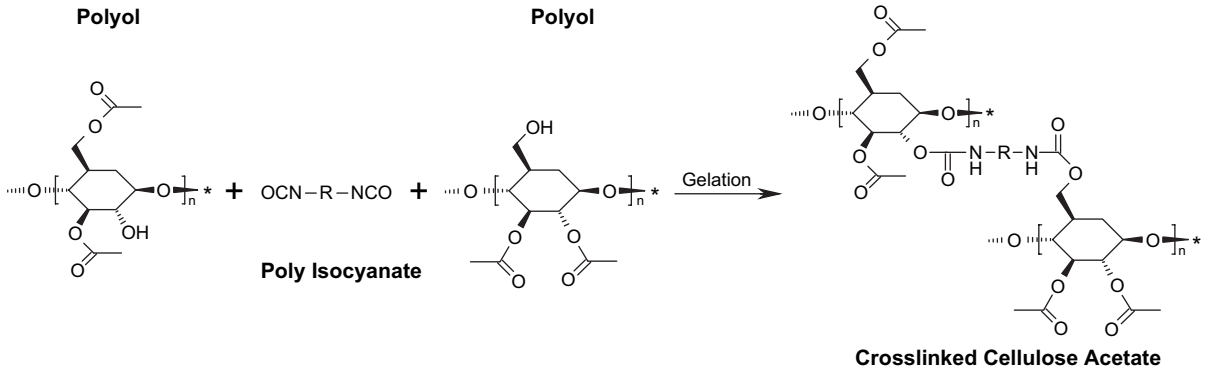

Fig. 1. Schematic of crosslinking by urethane bonding.

Table 1
Sol formulations, stoichiometric index (SI), gelation times (t_g) and syneresis shrinkages (τ_{syn})

	DP_n	%CA	CA/I	SI (%)	ρ_{sol} (g/cm^3)	ρ_{gel} (g/cm^3)	t_g (min)	τ_{syn} (%)
		±5%	±5%	±5%	±5%	±5%	±10%	±10%
OA1	190	10	1	270	0.150	0.188	15	20
OA2	190	10	5	66	0.100	0.100	20	0[a]
OA3	190	10	9	36	0.090	0.090	50	0[a]
OA4	115	5	1	270	0.080	0.125	60	36
OA5	115	5	11	27	0.045	0.045	150	0[a]

[a] Not significant.

Within the present study, in addition to the degree of polymerisation of the cellulose acetate, we have also varied the cellulose acetate concentration defined as the mass ratio between cellulose acetate and acetone indexed %CA (Eq. (1)), and the mass ratio between cellulose acetate and isocyanate, indexed CA/I (Eq. (2)). Resulting theoretical density in g/cm^3 is denoted as ρ_{sol} (Eq. (3)). Within the present study, %CA was equal to 5% or 10% while CA/I varied between 1 and 11 (Table 1).

$$\%\mathrm{CA} = \frac{m_{\mathrm{CA}}}{m_{\mathrm{acetone}}} \tag{1}$$

$$\mathrm{CA/I} = \frac{m_{\mathrm{CA}}}{m_{\mathrm{I}}} \tag{2}$$

$$\rho_{\mathrm{sol}} = \frac{m_{\mathrm{CA}} + m_{\mathrm{I}}}{V_{\mathrm{sol}}} \tag{3}$$

where m_{CA}, $m_{acetone}$, m_I are, respectively, the masses of cellulose acetate, acetone, isocyanate and V_{sol} is the volume of the sol (i.e. the volume of acetone used).

The gel density (ρ_{gel}) was calculated using the masses of reagents and gel volume and is calculated as follows (Eq. (4)):

$$\rho_{\mathrm{gel}} = \frac{m_{\mathrm{CA}} + m_{\mathrm{I}}}{V_{\mathrm{gel}}} \tag{4}$$

where V_{gel} is defined as the difference between V_{sol} and the volume of acetone expelled after syneresis is completed (i.e. seven days ageing).

2.3. Characterization

Gelation time (t_g) was defined as the duration between crosslinker introduction into the sol (mixing of solutions A and B in Fig. 2) and the instance at which no movement (non-flow of the sol) can be observed when the vial is tilted or inverted. It might be argued that such an experimental procedure to estimate t_g is quite empirical and could produce systematic errors compared to rheological characterisations. However, we have used for all formulations the same procedure, and we have verified systematically that the results were reproducible within an acceptable range.

Syneresis and drying shrinkages, respectively, denoted as τ_{syn} and τ_{scd} were expressed from the densities of the sol, gel and aerogel (i.e. obtained after supercritical CO_2 drying), and are calculated as in Eqs. (5) and (6).

$$\tau_{\mathrm{syn}} = 1 - \frac{\rho_{\mathrm{sol}}}{\rho_{\mathrm{gel}}} \tag{5}$$

$$\tau_{\mathrm{scd}} = 1 - \frac{\rho_{\mathrm{gel}}}{\rho_{\mathrm{b}}} \tag{6}$$

where ρ_{sol}, ρ_{gel} and ρ_b are, respectively, the densities of the sol, the gel and the aerogel.

Skeleton density (ρ_s) was measured through helium pycnometry [11] on a Micromeritics Accupyc 1330 apparatus. Bulk density (ρ_b) was determined by mercury pycnometry. Apparent porosity (ε) and global specific porous volumes (V_p) were calculated according to the following relations:

$$\varepsilon = 1 - \frac{\rho_{\mathrm{b}}}{\rho_{\mathrm{s}}} \tag{7}$$

$$V_{\mathrm{p}} = \frac{1}{\rho_{\mathrm{b}}} - \frac{1}{\rho_{\mathrm{s}}} \tag{8}$$

The internal texture was observed by scanning electron microscopy (SEM) with Jeol apparatus (JSM6330F) at 5 kV after coating the sample with a few nanometers of platinum. For the SEM investigations, cryo-fractures were realised at liquid nitrogen temperature (77 K).

Porosity was studied by mercury porosimetry. Measurements were performed on a Carlo-Erba 2000 porosimeter. Because mercury is not intruding the porous network, pore size distributions (PSD) were obtained with the buckling theory developed by Pirard et al. for hyperporous materials [12] (Eq. (9)). The buckling strength constant (k_f) used to compute PSD (from porous volume evolution during isostatic compression) was taken equal to 28 nm MPa$^{1/4}$ as previously established for similar materials [13].

$$L_{\mathrm{Hg}} = \frac{k_f}{P^{0.25}} \tag{9}$$

with L_{Hg} being the size of the largest pores remaining after compression at a pressure P.

Specific surface areas were determined through nitrogen sorption measurements on a Sorptomatic 1990 apparatus. BET surface (S_{BET}) was calculated over the relative pressure (P/P_0) range of 0.09–0.25 [14].

Finally, the effective thermal conductivity of the samples was measured with a CT-Meter apparatus using a technique based on the hot-wire method [15]. The measurements were performed at room temperature with the corresponding relative humidity, from secondary vacuum (10^{-8} bar) of air to atmospheric pressure. The absolute error is $\pm 0.5 \times 10^{-3}$ W/m K.

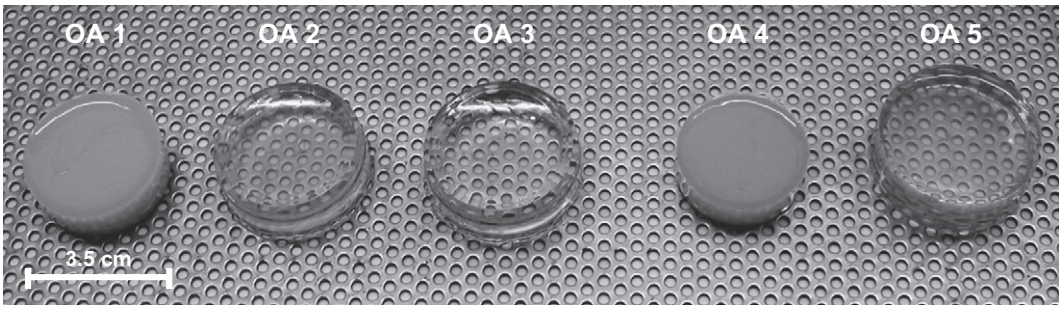

Fig. 3. Crosslinked cellulose acetate wet gels (according to formulations described in Table 1).

3. Results

3.1. Wet gels

All the investigated formulations lead to coloured monolithic gels as CA/I decreases (Fig. 3). Opaque gels are obtained with low CA/I values (OA1 and OA4) whereas translucent gels are prepared when CA/I is above 5 (OA2, OA3 and OA5). Gelation times range from some minutes to some hours and appear shortened when CA/I decreases. High-reticulated gels (CA/I = 1) undergo significantly larger syneresis shrinkage (Table 1).

We have defined stoichiometric index (SI) as the ratio between the amount of isocyanate introduced into the sol (m_I) and the calculated stoichiometric amount of isocyanate required to react with all hydroxyl groups of cellulose acetate (m_{IS}) (Eq. (10)). The isocyanate stoichiometric mass is calculated using cellulose acetate and crosslinker chemical characteristics, as illustrated in Eq. (11).

$$\mathrm{SI} = \frac{m_\mathrm{I}}{m_\mathrm{IS}} \tag{10}$$

$$m_\mathrm{IS} = \frac{m_\mathrm{CA} \times \mathrm{DP}_n \times \mathrm{DS}_\mathrm{OH} \times M_\mathrm{PMDI}}{f \times M_\mathrm{n}} \tag{11}$$

where M_{PMDI} is 374.4 g/mol, f is the average isocyanate functionality of PMDI equal to 2.8 and DS_{OH} is the substitution degree of cellulose acetate in hydroxyl groups equal to 0.6.

Using Eq. (11), the stoichiometric proportions (SI = 100%) are obtained for a theoretical CA/I ratio equal to 3.3. An SI value above 100% indicates that an excess of isocyanate was introduced during the synthesis in order to be sure to perform a complete crosslinking of the cellulose acetate.

Crosslinked polymers cannot dissolve in solvents because of the crosslinks between polymer chains. A classical method for measuring the Hildebrand parameter of such polymers (so-called screening procedure) is to immerse them into a series of solvent of different Hildebrand parameters (δ). The crosslinked material will swell at varying degrees, with the maximum swelling occurring when the solvent has the same Hildebrand parameter as that of the polymer [16,17]. Such solvency testing has been performed on our cellulose acetate crosslinked gels. After appropriate washing, wet gels have been immersed in different solvents (with different hydrogen bonding strength: poor, moderate or strong, and different δ). It has been observed that associated volume variation (shrinkage or swelling) of the gels was significantly influenced by the chemical nature of the solvent as illustrated in Table 2. In acetone, the gels have shown a maximal swelling while in hexane or heptane as well as in ethanol or 2-propanol, the gels underwent a high shrinkage. Thanks to this preliminary screening procedure with which we can estimate that the Hildebrand parameter of the present polymeric crosslinked gels ranges between 18.6 and 21.1 $MPa^{1/2}$.

3.2. Drying shrinkage, densities and apparent porosity

All the studied gels lead to monolithic, opaque and crack-free aerogels after supercritical CO_2 drying (Fig. 4). Whatever the formulation investigated the samples experienced high shrinkage during this step (τ_{scd}). Consequently, the global shrinkage (including both syneresis and drying steps) leads to relatively high bulk densities (ρ_b) and densification factor (F_D) (Table 3).

However, this shrinkage appears reversible when dry materials are immerged in synthesis solvent (i.e. acetone).

3.3. Elemental analysis

Elemental compositions of the synthesis precursors (cellulose acetate and isocyanate) and cellulose aerogel OA3 were determined at the Central Service of Analysis of CNRS

Table 2
Qualitative solvency testing of the gels

Solvent	Solubility parameter, δ ($MPa^{1/2}$)[a]	H-bonding group	Shrinkage of the crosslinked polymer[b]
Hexane	14.9	Poor	High
Heptane	15.1	Poor	High
Ethyl acetate	18.6	Moderate	Not significant
Methyl ethyl ketone	19.0	Moderate	Not significant
Acetone	20.3	Moderate	No shrinkage
Acetic acid	20.7	Strong	Not significant
Acetic anhydride	21.1	Strong	Not significant
2-Propanol	23.5	Strong	High
Ethanol	26.0	Strong	High

[a] Solubility parameter values from the polymer handbook 4th edition [17].
[b] As observed.

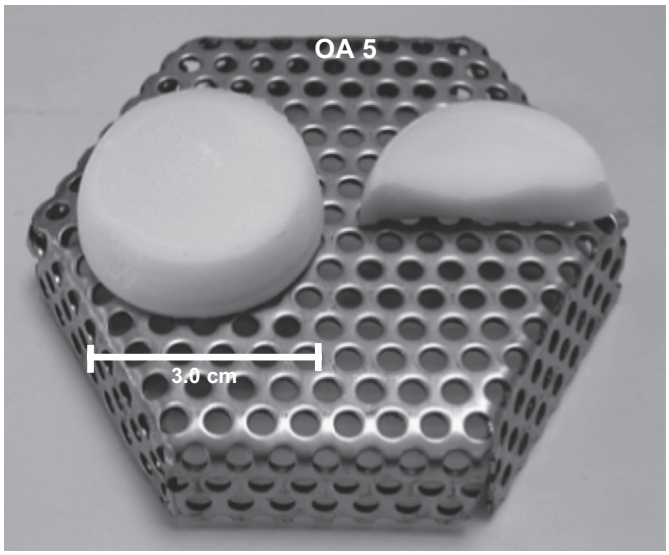

Fig. 4. View of OA5 sample.

Table 3
Drying shrinkage (τ_{scd}), apparent bulk density (ρ_b), densification factor F_D (equal to ρ_b/ρ_{sol}), skeleton density (ρ_s) and apparent porosity (ε)

	τ_{scd} (%)	ρ_b (g/cm^3)	F_D	ρ_s (g/cm^3)	ε (%)
	±5%	±10%	±10%	±1%	±5%
OA1	75	0.750	5.0	1.45	47
OA2	85	0.700	7.0	1.45	52
OA3	75	0.400	4.4	1.45	72
OA4	85	0.850	10.6	1.45	41
OA5	80	0.250	5.5	1.45	82

(Table 4). Experimental values measured for OA3 are compared to the theoretical values calculated using the precursors' compositions and the reagents' mass introduced during the sol–gel process. OA3 and OA3$_{theo}$ elemental compositions are identical, which means that all the isocyanate introduced react with the hydroxyl groups of cellulose acetate. This confirms that, as expected, the stoichiometry of OA3 reaction is not achieved (SI = 36%). Some tin traces are also detected in OA3. The tin quantity measured in the aerogel is due to the use of DD catalyst, certainly trapped in the nanoporous network. Based on these results, we have estimated that almost 20% of the initial mass of DD introduced during the gels synthesis is retained in the final dry material. Steric hindrance might explain why the tin complex remains in the porosity

Table 4
Elemental compositions of cellulose acetate aerogels OA3 and synthesis reagents (where % corresponds to the element mass in grams per 100 g of the material)

	PMDI (%)	Cellulose acetate (%)	OA3 (%)	OA3$_{theo}$ (%)
	±1%	±1%	±1%	±3%
%C	72.5	48.9	50.3	51.2
%O	12.1	45.3	42.6	42.1
%H	4.2	5.8	5.7	5.6
%N	11.2	–	1.1	1.1
%Sn	–	–	0.3	–

and cannot diffuse out of the gels during washing and drying steps. This observation encourages us, in the future, to test the non-metallic catalyst, especially if we consider our organic aerogels as the potential precursors for carbon aerogels [18]. Indeed, it is well-known that metals can act as poison and interfere with electrochemical reactions, for instance when carbon aerogels are used as electrodes of proton exchange membrane fuel cell.

3.4. Solid network

Solid backbone was also studied by SEM and nitrogen adsorption. Specific surfaces (calculated using the BET model) range from 150 to 250 m^2/g (Table 5). In parallel, for the whole set of formulations investigated, SEM showed a fibrillar solid network (Fig. 5). Moreover, it seems that the polymeric branches are formed by spheroid aggregates (like a pearl-necklace structure as observed in Fig. 5). Taking into account the spherical shape of the aggregates, BET values can be used in order to estimate the corresponding characteristic dimension of the solid aggregate (d_p) *via* simple geometric considerations (Eq. (12)). Corresponding values range

Table 5
Specific area (S_{BET}), average characteristic dimension of the solid aggregates (d_p), specific porous volume (V_p), partial specific porous volume investigated and fraction of porous volume investigated by mercury porosimetry (respectively, V_{Hg} and $\%V_{Hg}$, defined as V_{Hg}/V_p), characteristic porous size (L_{Hg}) estimated from the maximum of the PSD curve

	S_{BET} (m^2/g)	d_p (nm)	V_p (cm^3/g)	V_{Hg} (cm^3/g)	$\%V_{Hg}$ (%)	L_{Hg} (nm)
	±5%	±5%	±10%	±5%	±15%	±25%
OA1	230	18	0.65	0.50	77	13
OA2	160	26	0.75	0.70	93	12
OA3	140	30	1.80	1.80	100	22
OA4	210	20	0.50	0.40	80	12
OA5	250	17	3.30	3.30	100	25

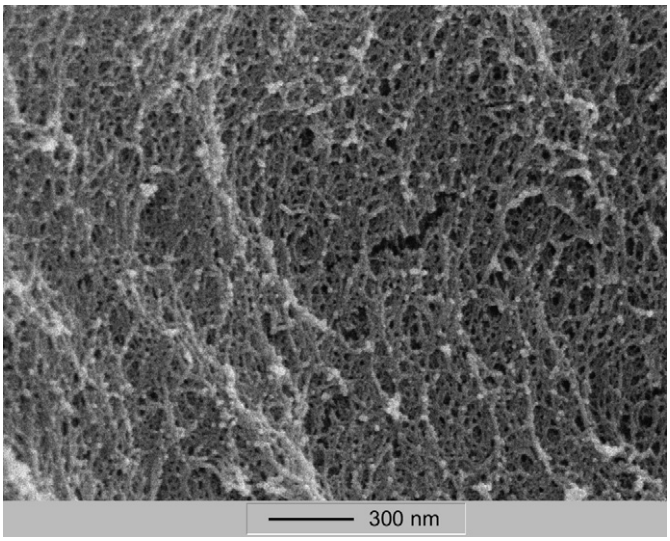

Fig. 5. SEM micrograph of cellulose acetate aerogels OA5.

between 15 and 30 nm, which seem to be in good accordance with the SEM micrographs.

$$d_p = 6\frac{V_s}{S_{BET}} \quad (12)$$

with V_s being the specific solid volume (taken equal to $1/\rho_s$).

3.5. Specific volumes and pore size distributions

Partial specific porous volumes measured by mercury porosimetry (V_{Hg}) appeared relatively close to the ones calculated from apparent and skeleton densities (V_p). Most of the porous volume is characterised by this method ($\%V_{Hg}$ superior to 77%). The remaining volume is due to the smallest pores, with average diameter under the detection limit of mercury porosimetry (i.e. 7.5 nm).

The PSD of the aerogel (obtained using mercury porosimetry results treated with Pirard et al. theory [12,13]) are illustrated in Figs. 6 and 7. Associated to the fact that $\%V_{Hg}$ is high (Table 5), they clearly indicate that the five aerogels obtained are mainly mesoporous (i.e. the mercury porous volume measured (V_{Hg}) is only due to the contribution of pores with characteristic diameters in the range of 2–50 nm). Besides, the mean pore diameter (L_{Hg}) is dependent on the formulation used.

3.6. Mechanical properties

Compressive behaviour of the cellulose acetate aerogels was studied through the bulk modulus K [19], defined as the

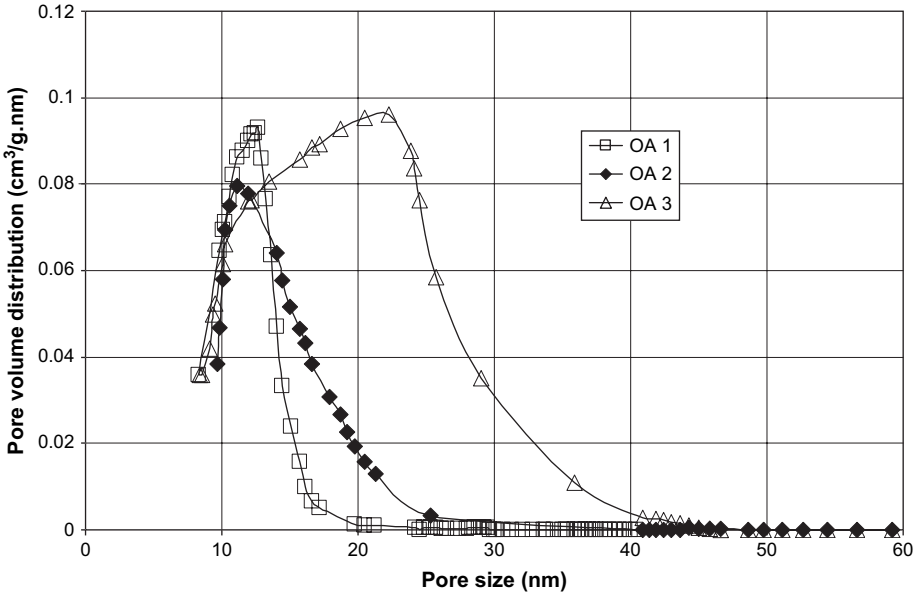

Fig. 6. Pore-size distributions determined by mercury porosimetry for cellulose acetate aerogels (DP_n equal to 190, 10%CA).

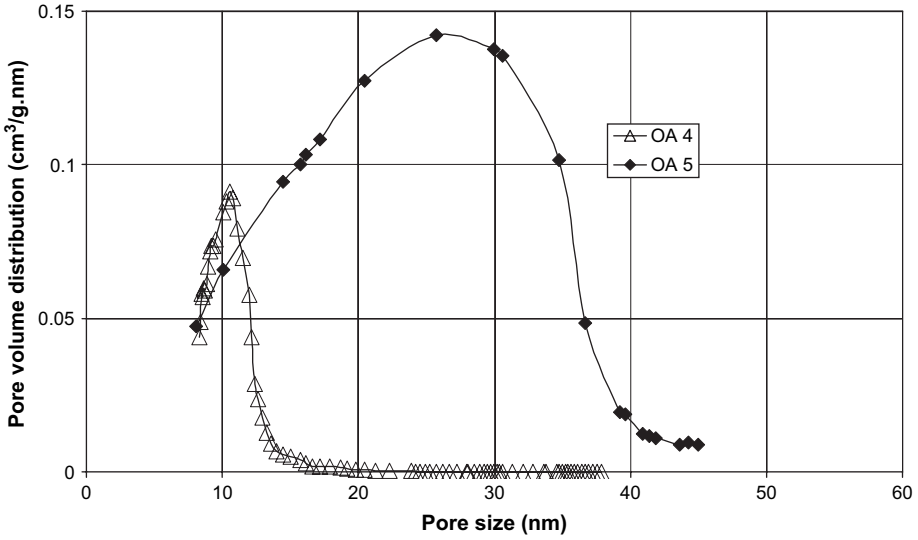

Fig. 7. Pore-size distributions determined by mercury porosimetry for cellulose acetate aerogels (DP_n equal to 115, 5%CA).

"constant" relating the applied pressure (P) and the volumetric strain ($\Delta V/V$) (Eq. (13)).

$$\Delta P = K\frac{|\Delta V|}{V} \tag{13}$$

The initial modulus K was calculated in the early stages of mercury compression as follows (Eq. (14)):

$$K = \frac{1}{\rho_b}\beta \tag{14}$$

where ρ_b is the bulk density (g/cm^3) and β (in MPa g/cm^3) is the mean slope of the mercury porosimetry curve (pressure P *versus* volume variation ΔV) in the linear early compression stages when $P < 1$ MPa.

Young's modulus E (MPa) was then derived from K using a standard proportionality rule (Eq. (15)).

$$E = 3(1-2\nu)K \tag{15}$$

in which Poisson's ratio ν is taken equal to 0.4 for cellulose acetate materials [20].

Results are summarised in Table 6. Cellulose acetate aerogels experience K-values of the same order of magnitude as RF aerogels [21]. K modulus increases as a function of bulk density ρ_b. The linear log–log plot follows the typical aerogels power-law density $K = K_0\rho^{\alpha}$ [22] with an α-exponent equal to 3.3 ± 0.3 (Fig. 8). Furthermore, like RF aerogels [23], mechanical behaviour of the samples is significantly influenced by the formulation. Whatever %CA be, K is increasing with SI.

Table 6
Bulk and Young's modulus (K and E) of cellulose acetate aerogels

	ρ_b (g/cm^3)	K (MPa)	E (MPa)
	±10%	±50%	±50%
OA1	0.75	338	203
OA2	0.70	142	85
OA3	0.40	14	8
OA4	0.85	472	283
OA5	0.25	11	7

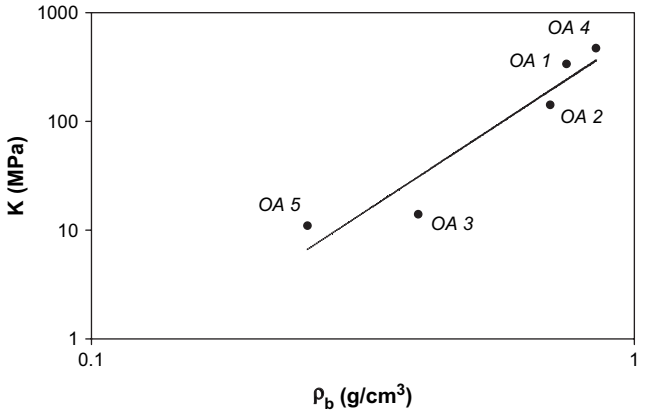

Fig. 8. Bulk modulus (K) *versus* bulk density (ρ_b) of cellulose acetate aerogels (with dash line representing the power-law density $K = K_0\rho^{3.3}$).

3.7. Thermal conductivity

Effective thermal conductivity has been characterised at room temperature on granular beds with particle size distribution between 0 and 3 mm (Fig. 9). Evolution of conductivity with partial vacuum has been measured from secondary vacuum (10^{-8} bar) to atmospheric pressure (Fig. 10). Results obtained on cellulose acetate aerogels have been compared with standard micrometer-sized insulating material (monolithic polyurethane foam) and also with nanostructured and nanoporous super-insulating material (granular bed of silica xerogel with similar particle size distribution [24]). Effective thermal conductivity ranges from 0.029 W/m K (at atmospheric pressure) to 0.006 W/m K (at 2×10^{-5} mbar) and stands

Fig. 9. View of a 600 cm^3 bed of granular cellulose acetate aerogel (hot-wire immerged in a divided OA5 bed).

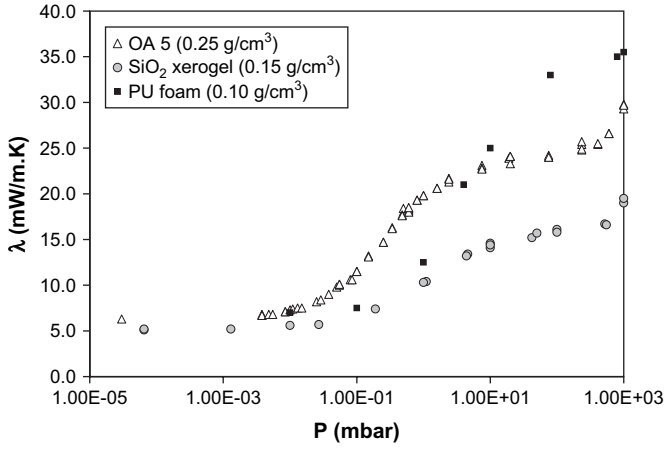

Fig. 10. Effective thermal conductivity of OA5 cellulose acetate aerogel *versus* pressure and comparison with commercial polyurethane foam and divided silica xerogel.

in-between polyurethane foam and divided silica xerogel in the primary vacuum range.

4. Discussions

4.1. Drying shrinkage

All the investigated cellulose acetate gels undergo a very large shrinkage during supercritical CO_2 drying ($\in$ [75%; 85%]). For instance, the average diameter of OA5 gel is about 4 cm before drying (Fig. 3) and decrease to about 3 cm after drying (Fig. 4). This linear shrinkage estimated at 25% can be extrapolated to a volume shrinkage of 60% (in the hypothesis of an ideal isotropic shrinkage which leads to the same contraction in the height of the aerogel). The shrinkage measured ($\tau_{scd} \approx 80\%$) is higher, which may be due to the non-isotropy of the contraction. As seen in Fig. 4, the thickness of the border of the aerogel monolith might be slightly higher than the thickness of the center of the monolith. In fact, mercury pycnometry has evaluated the global density of the material (by weighting the mass of a representative piece of the sample and measuring its corresponding volume), which takes into account the non-homogeneity of the material.

This shrinkage does not result from mechanical stress. Indeed, compared to evaporative drying, the supercritical route is well-known to vanish capillary tension [25] when operated above the critical point of the mixture contained in the porosity [26] (which is the case according to the binary CO_2–acetone phase diagram presented in Fig. 11; we have verified that such an operating pressure is above the critical pressure of the mixture at 40 °C) and when depressurisation is performed – as present – safely regarding to eventual tensile stress related to low gels permeability [28]. Besides, operating temperature (40 °C) is far enough from the glass transition range of the generated polymeric network to avoid partial melting which can induce a volume variation.

Consequently, the observed shrinkage may only come from interactions between gels and CO_2 [29]. Indeed, replacing initial interstitial solvent (acetone) by a different one (CO_2) forces the gels to reach another equilibrium state which mainly depends on its chemical affinity with CO_2 as well as the elasticity of the solid network [30]. Generally, no significant shrinkage is observed for inorganic gels like silica the ones contrary to their much more elastic organic counterparts (RF, melamine formaldehyde, polyurethane, …).

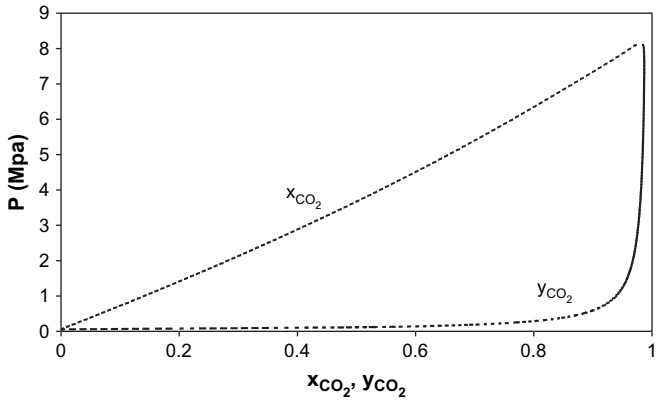

Fig. 11. CO_2–acetone equilibrium phase at 40 °C calculated from Chang et al. measurements [27] with Redlich–Kwong equation of state used with predictive Soave–Redlich–Kwong mixing rules (x_{CO_2} and y_{CO_2} represent, respectively, CO_2 molar fraction in the liquid and the gas phases). Critical pressure appears close to 81.5 bars.

Calculation of Hildebrand parameter of CO_2 in the operating supercritical conditions (80 bars and 40 °C) leads to a δ-value of 4.9 $MPa^{1/2}$ (Eq. (16)) [16]. Comparison of this value with that of the screening results obtained on the gels (Table 2) is consistent with the high shrinkage ratio occurring during the drying step (Table 3). This statement appears consistent with post-drying shrinkage reversibility in acetone.

$$\delta = \left(1.25 P_c^{1/2}\right) \frac{\rho_r}{\rho_{r,l}} \tag{16}$$

with P_c (critical pressure), ρ_r (reduced density of the supercritical fluid) and $\rho_{r,l}$ (reduced density of the liquid) respectively, equal to 73.8 bars, 0.605 and 2.7 g/cm^3 for CO_2. δ is obtained in $(cal/cm^3)^{1/2}$ using Eq. (16).

4.2. Influence of the crosslinking ratio

The DD-catalysed samples undergo roughly identical drying shrinkages ($\tau_{scd} = 80\% \pm 5\%$) for the investigated formulations. Consequently, influence of the sol–gel formulation can be discussed on the basis of the dried samples assuming that the drying step induces similar impact on all the wet gels.

The results have shown that, whatever the cellulose acetate concentration (%CA = 5 or 10) be, the CA/I parameter has a strong influence, especially in terms of kinetics of gelation and texture of the aerogel. First of all, decreasing CA/I speeds up the gelation process. A lower crosslinker concentration is leading to a slower sol–gel transition. Secondly, it was observed that stoichiometric proportions (SI $\geq$ 100%) induce larger syneresis shrinkages. In fact, this observation could be directly related to the increase of the degree of reticulation of the cellulose acetate macromolecules *via* the augmentation of the crosslinker concentration. Associated to the facts that varying the crosslinking ratio CA/I seems to have no significant influence on drying shrinkage and that, at constant %CA, it implies an augmentation of ρ_{sol}, this syneresis shrinkage leads to an increase of the densification factor (F_D) and the bulk density (ρ_b). Furthermore, because skeleton density (ρ_s) appears independent of CA/I, according to Eqs. (3) and (4), the ρ_b augmentation results in a strong decrease of porosity (ε) and specific porous volume (V_p). This behaviour is logically accompanied by a contraction of the mercury PSD towards the lower pore sizes zone (Figs. 6 and 7) and by a reduction of the characteristic pore dimension (L_{Hg}) determined by mercury porosimetry. Besides, decreasing CA/I is also suspected to create small pores, presenting dimensions lower than the detection limit of the present method (i.e. 7.5 nm). Indeed, at low reticulation ratio, the porous volume is fully characterised ($\%V_{Hg} = 100$ for samples OA3 and

OA5) while for lower CA/I values $\%V_{Hg}$ tends to diminish drastically (Table 5).

Contrary to the porous network, no clear influence of CA/I on the solid network can be set off at present. Indeed, the influence of CA/I on specific area (S_{BET}) and derived average aggregate size (d_p) seems to depend on %CA. For concentrated sols (%CA = 10, samples OA1, OA2 and OA3), the decrease of CA/I is accompanied by an increase in specific area (S_{BET}). Such an evolution is representative of a textural refinement illustrated by the diminution of the characteristic size of the objects constituting the solid skeleton (Table 5). The opposite tendency seems to be observed with diluted sols (%CA = 5, samples OA4 and OA5).

4.3. Thermo-mechanical properties

Tan and co-workers have underlined the mechanical interest of cellulose-based aerogels [8], insisting particularly on their high impact strength (10 times larger than that of RF aerogels). Within the present study, no particular difference between cellulose acetate and RF aerogels can be observed regarding to compression (as illustrated by *K*-values of the same order of magnitude).

Effective thermal conductivity follows standard evolution of granular beds with partial vacuum [31]. At lowest pressure (10^{-5}–10^{-2} mbar), radiative transfer and solid conduction govern thermal transfer. The increase in conductivity at intermediate low-pressure (approximately from 10^{-2} to 10 mbar) comes from gas conduction in voids between aerogel granules. Finally, the atmospheric λ-increase is caused by gas conduction in mesopores within the granules. Comparison with divided silica xerogels sets off identical behaviour but significantly larger values as soon as gas conduction arises. This is partly due to less finer nanostructuration of the internal porosity.

5. Conclusions

Nanostructured and mesoporous materials have been elaborated *via* sol–gel crosslinking of cellulose acetate with a non-toxic isocyanate followed by supercritical carbon dioxide drying.

It has been demonstrated that the crosslinker content has an important impact on both gelation and aerogels properties, whatever cellulose degree of polymerisation and concentration be. Varying its concentration in solution has shown it is possible to modify bulk density, porous volume and pore size distribution of the final materials.

It has also been observed that this type of gels undergoes large shrinkage during supercritical carbon dioxide drying. Thanks to Hildebrand parameter analysis, such a shrinkage has been related to poor chemical affinity between crosslinked polymer network and supercritical carbon dioxide. This result has been confirmed by the reversibility of the shrinkage after re-wetting of the dry materials in acetone.

On the basis of these correlations, a low-density (0.25 g/cm^3) and highly mesoporous (3.30 cm^3/g) material has been prepared.

To go further, divided cellulose-based aerogels were studied as ''green'' materials for thermal insulation application. They have shown promising low thermal conductivity at atmospheric pressure (inferior to 0.030 W/m K) comparable with that of typical insulating foams (like polyurethane). However, first thermal conductivities are higher than super-insulating materials like silica aerogels.

Further optimisations will be performed in order to decrease the density of our cellulose-based aerogels while preserving nanostructuration and to avoid the presence of metallic compounds that remain trapped in the network.

Acknowledgements

The authors are grateful for financial support from the European Commission (European FP6 project AEROCELL, contract 50588-1). They also gratefully acknowledge Pierre Ilbizian (ARMINES/ENSMP/CEP/EM&P) for supercritical CO_2 drying, Christophe Coquelet (ARMINES/ENSMP/CEP/TEP) for CO_2–acetone phase diagram and Manfred Pinnow (FhG-IAP-Natural polymer division) for the scanning electron micrograph.

References

[1] Hüsing N, Schubert U. Ullmann's encyclopedia of industrial chemistry. 6th ed. Wiley; 2002.
[2] Pekala RW. J Mater Sci 1989;24:3921.
[3] Biesmans G, Randall D, Francais E, Perrut M. J Non-Cryst Solids 1998; 225:36.
[4] Rigacci A, Marechal JC, Repoux M, Moreno M, Achard P. J Non-Cryst Solids 2004;350:372.
[5] Jin H, Nishiyama Y, Wada M, Kuga S. Colloid Surf A Physicochem Eng Asp 2004;240:63.
[6] Weatherwax RC, Caulfield DF. TAPPI J 1971;54:985.
[7] Pimenov VG, Drozhzhin VS, Sakharov AM. Polym Sci Ser B 2003;45:4.
[8] Tan C, Fung B, Newman JK, Vu C. Adv Mater 2001;13:644.
[9] Dieterich D, Uhlig K. Ullmann's encyclopedia of industrial chemistry. 5th ed. Wiley; 1996.
[10] Bisson A, Rigacci A, Lecomte D, Rodier E, Achard P. Dry Technol 2003; 21:593.
[11] Ayral A, Phalippou J, Woignier T. J Mater Sci 1992;27:1166.
[12] Pirard R, Blacher S, Brouers F, Pirard JP. J Mater Res 1995;10:2114.
[13] Pirard R, Rigacci A, Marechal JC, Quenard D, Chevalier B, Achard P, et al. Polymer 2003;44:4881.
[14] Gregg SJ, Sing KSW. Adsorption, surface area and porosity. 2nd ed. London: Academic Press; 1982.
[15] Lu X, Nilsson O, Fricke J, Pekala RW. J Appl Phys 1993;73:581.
[16] Barton AFM. Handbook of solubility parameters and other cohesion parameters. 2nd ed. CRC Press; 1991 [chapter 14].
[17] Brandrup J, Immergut EH, Grulke EA. Polymer handbook. 4th ed. Wiley; 1999 [chapter 8].
[18] Fischer F, Guilminot E, Chatenet M, Rigacci A, Berthon-Fabry S, Chainet E, et al. In: Proceedings of the seventh European symposium on electrochemical engineering, Toulouse, France; October 3–5, 2005.
[19] Scherer GW, Smith DM, Qui X, Anderson JM. J Non-Cryst Solids 1995; 186:316.
[20] Le Neindre B. Coefficient d'élasticité, K486, Traité constantes physico-chimiques, Techniques de l'ingénieur, Paris; 1991.
[21] Pekala RW, Alviso CT, LeMay JD. J Non-Cryst Solids 1990;125:67.

[22] Ma HS, Prévost JH, Jullien R, Scherer GW. J Non-Cryst Solids 2001;285: 216.
[23] Gross J, Scherer GW, Alviso CT, Pekala RW. J Non-Cryst Solids 1997; 211:132.
[24] Bisson A, Rigacci A, Lecomte D, Achard P. J Non-Cryst Solids 2004; 350:379.
[25] Pierre AC, Pajonk GM. Chem Rev 2002;102:4243.
[26] Van Bommel MJ, De Haan AB. J Mater Sci 1994;29:943.
[27] Chang CJ, Day CY, Ko CM, Chiu KL. Fluid Phase Equilib 1997;131:243.
[28] Woignier T, Scherer GW, Alaoui A. J Sol–Gel Sci Technol 1994;3:141.
[29] Tanaka T. Sci Am 1981;244:124.
[30] Phalippou J, Kocon L, Aérogels. Aspects fondamentaux, AF 3609, Techniques de l'ingénieur, Paris; 2004.
[31] Fricke J, Hümmer E, Morper HJ, Scheuerpflug P. In: Proceedings of the second international symposium on aerogels ISA2, Montpellier, France; September 1989.